ISSN 0027-1349, Moscow University Physics Bulletin, 2013, Vol. 68, No. 5, pp. 387–396. © Allerton Press, Inc., 2013.
Original Russian Text © V.B. Zaitsev, E.A. Konstantinova, D.M. Deygen, M.N. Rumyantseva, E.V. Podol'ko, M.V. Pustovalov, P.K. Kashkarov, 2013, published in Vestnik Moskovskogo Universiteta. Fizika, 2013, No. 5, pp. 49–57.

The Optoelectronic Properties of Nitrogen- and Carbon-Doped Nanocrystalline Titania

V. B. Zaitsev[a], E. A. Konstantinova[a, b], D. M. Deygen[a], M. N. Rumyantseva[c], E. V. Podol'ko[c], M. V. Pustovalov[c], and P. K. Kashkarov[a, b]

[a] *Department of General Physics and Molecular Electronics, Faculty of Physics, Moscow State University, Moscow, 119991 Russia*

[b] *Russian Research Center, Kurchatov Institute, pl. Akademika Kurchatova 1, Moscow, 123182 Russia*

[c] *Department of Inorganic Chemistry, Faculty of Chemistry, Moscow State University, Moscow, 119991 Russia*

e-mail: vzaitsev@phys.msu.ru; liza35@mail.ru; d.m.deygen@gmail.com; roum@inorg.chem.msu.ru; suhofrukt91@mail.ru; xnastyx@bk.ru; pavel@vega.phys.msu.ru

Received July 3, 2013; in final form June 19, 2013

Abstract—Carbon- and nitrogen-doped nanocrystalline titania specimens were studied by optical spectroscopy and electron paramagnetic resonance. The doping of this material was established to result in the appearance of additional absorption in the visible spectral region. The doping with admixture nitrogen was revealed to lead to the formation of nitrogen-containing paramagnetic sites, namely, N• and NO• radicals. The effect of the recharging of the detected sites under light was revealed. The obtained results could be useful for the development of photocatalytic filters on the basis of doped nanocrystalline titania.

Keywords: nanocrystalline titania, EPR spectroscopy, paramagnetic sites, doping.

DOI: 10.3103/S0027134913050160

INTRODUCTION

In recent years, studies of the physicochemical properties of titania nanoparticles obtained by different methods have become a frequent practice [1–4]. The given material is characterized by high chemical activity under ultraviolet radiation (UV) and this allows its use as reaction catalysts [5, 6], as an active component of solar cells [7, 8], etc. As is known, the activity of TiO_2 nanoparticles is much higher in comparison with the bulk material due to its increased active surface area.

The UV radiation of titania nanoparticles leads to the generation of electron–hole pairs that participate in the catalytic processes on the surface of particles due to the absorption of photon energy. The process is generally accompanied by the inverse phenomenon, i.e., the recombination of charge carriers. The probability of the recombination of electron–hole pairs was established to depend on the bandgap energy (E_g) of a semiconductor [9]. The higher E_g is, the lower the probability of the transition of electrons from the conduction band into the valence band is. On the other hand, the use of semiconductors with a low E_g allows the useful energy to be increased for TiO_2 under solar radiation, as the excitation of valence-band electrons requires lower-energy photons [10]. In this connection, studies devoted to revealing factors that have an effect on the change of the bandgap energy of nanoparticles become topical. Titania is a wide-bandgap semiconductor with an E_g of nearly 3–3.3 eV, which allows us to use the absorption spectrum of TiO_2 nanoparticles for the estimation of E_g at the intrinsic absorption edge [11].

The objective of our work is to obtain TiO_2 nanoparticles doped by different methods and to perform the further analysis of their spectral characteristics with the purpose of determining the changes introduced into the absorption spectra of nanoparticles in the course of their modification.

SYNTHESIS OF SPECIMENS

Nanoparticles were obtained by the sol-gel method, which includes the preparation of a sol with its subsequent transition into a gel, i.e., into a colloid system consisting of a liquid disperse medium confined within a spatial network formed by linked disperse-phase particles [12–19]. The sol-gel method is a universal process that is used to obtain inorganic nanocrystalline materials. The sol-gel process occupies a special niche among the chemical methods for the synthesis of nanomaterials due to the possibilities of the fine control of target product properties, the flexible variation of synthesis conditions, and also due to low requirements for the purity of the reagents and a broad spectrum of chemical and physical modification. This method can be applied for the synthesis of almost all the types of doped TiO_2. The wide applica-

The sizes of nanocrystalline titania nanocrystallites according to the method of X-ray diffraction

Specimen	d, nm ± 1
C-TiO_2-1 (0.2 wt % of C)	15
C-TiO_2-2 (0.4 wt % of C)	17
C-TiO_2-3 (1 wt % of C)	17
N-TiO_2-1 (0.2 wt % of N)	15
N-TiO_2-2 (0.4 wt % of N)	12
N-TiO_2-3 (1 wt % of N)	12

tion of this method is due to a number of reasons. In the first instance, this is its universality, as was already mentioned above. Then, this method is easy to implement and does not require expensive equipment. It should also be noted that the sol-gel method is based on readily feasible hydrolysis chemical reactions, most of which are rather fast.

Nanocrystalline titania was synthesized as follows. To a concentrated hydrochloric acid solution, titanium tetrachloride was added until 15 wt % of $TiCl_4$ was attained. A 25% ammonia solution (56 mL; density, 0.9 g/mL) was then added to the obtained solution drop by drop under continuous stirring, whereupon a white flake-like precipitate was observed to form by the reaction

$$H_2TiCl_6 + 6NH_3 \cdot H_2O = 6NH_4Cl + TiO_2 \cdot xH_2O\downarrow + (4 - x)H_2O.$$

The resulting precipitate was repeatedly washed from chlorine ions by the method of sequential centrifugation and decantation. The precipitate was separated out by centrifugation and divided into several portions: the first portion was dried in a drying cabinet at 100°C for a day and the second portion was allowed to stay in the form of a suspension. The dried powder was ground in an agate mortar and then subjected to thermal annealing in air at a temperature of 300°C for a day. This is the method by which the non-doped nanocrystalline titania used in reference experiments was synthesized.

Nitrogen-doped nanocrystalline titania was synthesizes as follows. To introduce nitrogen into the structure of titania, a synthesized titanic acid suspension was boiled with an ammonium carbonate $(NH_4)_2CO_3$ solution with a reflux condenser for 3 h. To obtain specimens with different nitrogen admixture concentration, we used various ratios of a titanic acid suspension and an $(NH_4)_2CO_3$ solution. The $NTiO_2$ (0.2 wt %), $NTiO_2$ (0.4 wt %), and $NTiO_2$ (1 wt %) specimens were synthesized using the following reagent ratios: 20 g of ammonium carbonate in 100 mL of water, 35 g of ammonium carbonate in 100 mL of water, and 75 g of ammonium carbonate in 100 mL of water, respectively. The obtained white precipitate was separated out by centrifugation and annealed in air at a temperature of 300°C for a day.

Carbon-doped nanocrystalline titania was synthesized as follows. To an H_3TiCl_6 hydrochloride acid solution (30 mL, 15 wt % of $TiCl_3$), $NH_2OH \cdot HCl$ was added until the violet color disappeared. The resulting solution was diluted with water in such a fashion that the concentration of $TiCl_4$ was 0.25 M. The solution was then cooled with ice with the simultaneous dropwise addition of TBA (0.25 M) in the stoichiometric amount. The level of pH was nearly 2. The stoichiometry was calculated by the following reaction:

$$H_2TiCl_6 + 2(n\text{-}Bu)_4N^+OH^- \longrightarrow [TiCl_4(H_2O)_2] + 2(n\text{-}Bu)_4N^+Cl^-.$$

The remaining TBA solution was added to the mixture until the level of pH = 3 was attained. An NH_3 solution was then added to increase the level of pH to 5.5. The suspension was allowed to stay for 24 h for aging. The suspension was then centrifuged and the precipitate was dried at 70°C for 3 days.

The dried powder was ground in a mortar for 30 min. The obtained powder was annealed for 1 h at 400°C and a heating rate of 5°C/min. After annealing, the powder was ground once again. The obtained specimens had a carbon concentration of 0.2 wt % ($CTiO_2$). In the other variant, the remaining TBA solution was added to the $TiCl_4$–TBA mixture until the level of pH = 4 was attained. Further treatment was performed in the same way as in the first variant. Thus, synthesized specimens had a carbon concentration of 0.4 wt% ($CTiO_2$). In the third variant, the remaining TBA solution was added to the mixture until the level of pH = 5 was attained at the initial stage. The obtained specimens had a carbon concentration of 1 wt % ($CTiO_2$).

For our study, we prepared TiO_2 powder specimens (pure TiO_2 powder prepared in two different reactions, four types of TiO_2 powders doped with nitrogen to various degrees, and three types of TiO_2 powders doped with carbon to various degrees). The specimens were prepared on substrates of the two types: transparent and completely absorbing visible and UV radiation substrates (three specimens of each type on each substrate).

METHODS OF STUDIES

The microphotos of specimens were taken with using an Leo912 AB Omega transmission-electron microscope.

The diffuse scattering spectra of the obtained specimens were studied on a Perkin Elmer LS-55 spectrograph. The instrument allows the detection of the diffuse scattering of light from the surface of specimens in the spectral region of 200–900 nm with a spectral slit width from 2.5 to 20 nm.

The paramagnetic sites (radicals) were studied on a Bruker Elexsys-500 EPR spectrometer (operational frequency, 9.5 GHz; instrument sensitivity, 5×10^{10} spin/Gs). To calculate the concentration of para-

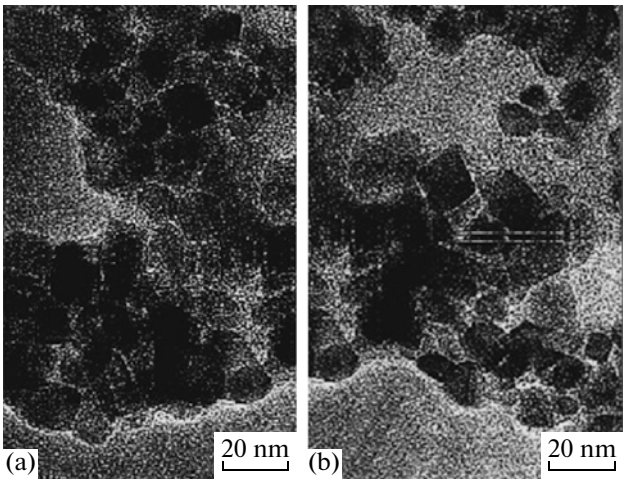

Fig. 1. Microphotos of nanocrystalline titania doped with (a) nitrogen and (b) carbon.

magnetic sites, we used a reference specimen ($CuCl_2 \cdot 2H_2O$) with a known number of spins. The procedure of determining the concentration of paramagnetic sites with the use of reference specimens is standard and has been described in many works, for example, in [20]. The temperatures of the measurements were 300 and 110 K.

The microstructure of the materials was studied by transmission electron microscopy (TEM) on a Leo912 AB Omega microscope (Center of Collective Use, Moscow State University). The accelerating voltage was 100 kV, the image resolution was 0.2 nm, the magnification was 80–500 000 times. Small amounts of powders were placed onto gold grids coated with a thin polymer film.

EXPERIMENTAL RESULTS

As follows from the results of transmission electron microscopy (Figs. 1a and 1b), the studied materials contain spherical irregularly shaped nanocrystals.

To determine the size of nanoparticles with a higher precision, we used the method of X-ray diffraction. The size of nanocrystallites (coherent scattering regions) was estimated from the broadening of diffraction reflections by the Scherrer's equation

$$d_{XRD} = \frac{k\lambda}{\beta\cos\theta},$$

where d_{XRD} is the average size of a coherent scattering region, β is the full width at the half maximum for the corresponding diffraction peak, λ is the radiation wavelength, θ is the diffraction angle, and $k = 0.9$. To obtain X-ray diffraction patterns, we studied the powder specimens on a Dron 4M X-ray diffractometer at room temperature under the following conditions: X-ray wavelength, 1.5406 Å, diffraction angle range of measurements, 10–70 deg; step, 0.05 deg; time of signal accumulation at each point, 5 s. The size of crys-

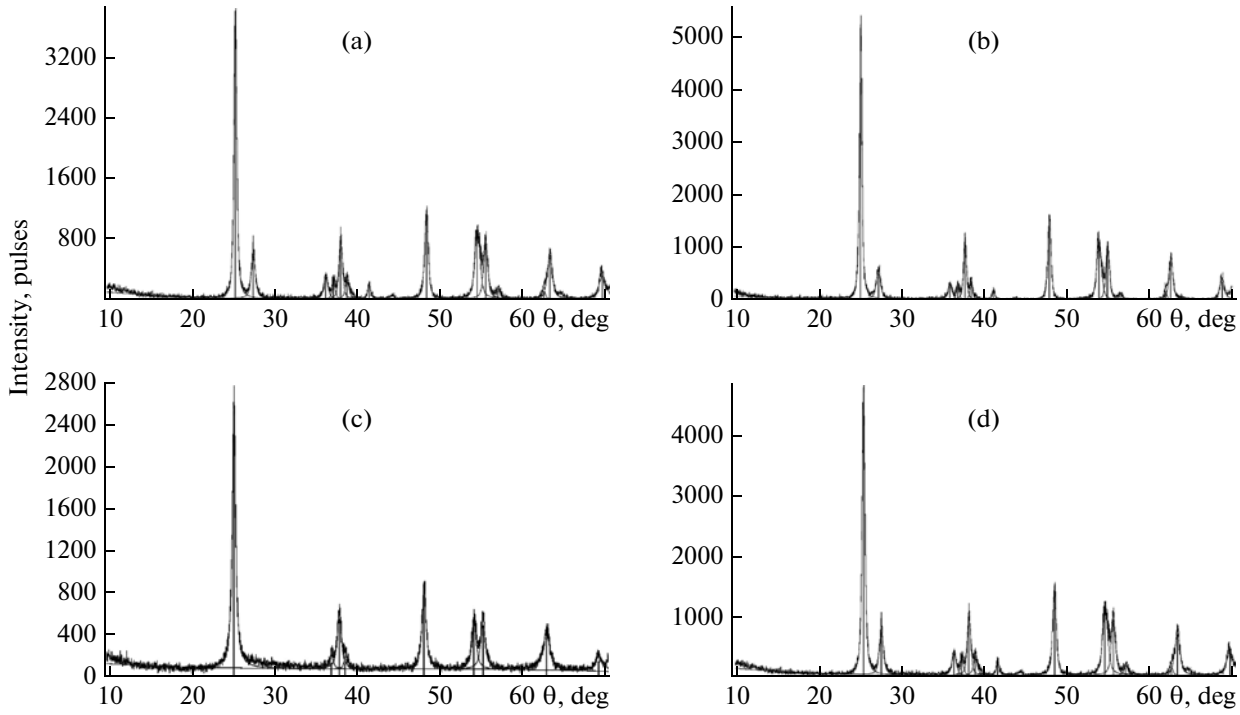

Fig. 2. X-ray diffraction patterns of (a) N–TiO_2–1, (b) N–TiO_2–3, (c) C–TiO_2–1, and (d) C–TiO_2–3 specimens.

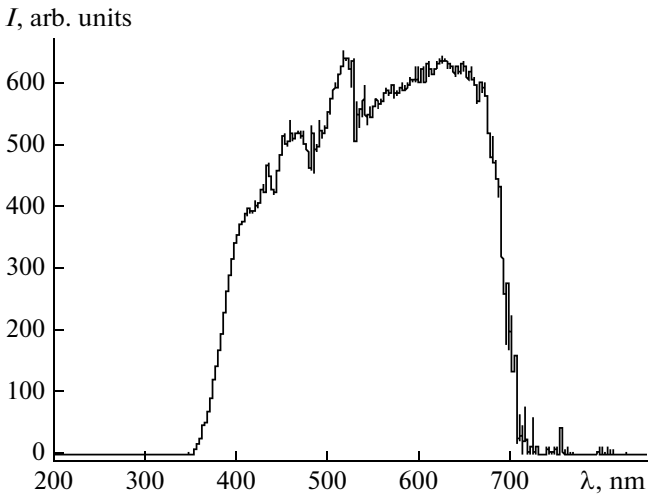

Fig. 3. The light-scattering spectrum of a pure TiO_2 specimen in the region from 200 to 850 nm.

tallites (coherent scattering regions) was determined by the Scherrer's equation using Grain software. Only the coherent scattering region sizes calculated for the three most intense diffraction peaks were taken into account. The obtained values were rounded off to whole nanometers with allowance for the model error. The relative error of the estimation method was 10%. The X-ray diffraction patterns of doped nanocrystalline titania specimens with minimum and maximum concentrations of admixture nitrogen and carbon are shown in Fig. 2.

The results of estimating the size of titania crystallites by X-ray diffraction are given in the table.

On the basis of the above, it is possible to make the following conclusions:

(1) The size of nanocrystallites in doped nanocrystalline titania specimens varies within a range from 10 to 20 nm; and

(2) The specific surface area of doped nanocrystalline titania specimens lies within a range from 10 to 20 nm.

The typical appearance of the light scattering spectrum of a pure TiO_2 specimen we synthesized in the region from 200 to 850 nm is shown in Fig. 3.

The optical bandgap energy E_g of TiO_2 nanopowders was determined at the so-called intrinsic absorption edge. Several methods exist to accomplish this.

The first method allows us to make an approximate estimate of E_g. To perform this, it is necessary to plot the dependence of the absorption coefficient α on the wavelength λ of incident light using a light scattering spectrum. The plot must have a shape similar to that shown in Fig. 4a.

In reality, the energy of a light quantum is related with the wavelength as

$$E_I = \frac{hc}{\lambda},$$

where h is Planck's constant and c is the speed of light. Moreover, $E_I = \hbar\omega = h\nu$. At high λ, the energy of a quantum is small and absorption is absent. This corresponds to the right part of the curve shown in Fig. 4a. Once λ attains the value of λ_{edge},

$$\Delta E = \frac{hc}{\lambda_{edge}},$$

the absorption begins to abruptly grow. This means that a sharp kink of the $\alpha(\lambda)$ dependence occurs at $\lambda = \lambda_{edge}$ (see Fig. 4a).

The difficulty of this approach consists in the correct estimation of the absorption coefficient from scattering spectra. The value of α of semiconducting materials varies within a wide range from 10^{-2} to 10^5 cm^{-1}. For this reason, when the absorption coefficient is measured, the thickness of a specimen is selected in such a fashion that the absorbance $D = \alpha d$ (where d is the thickness of a specimen) is nearly 1. In

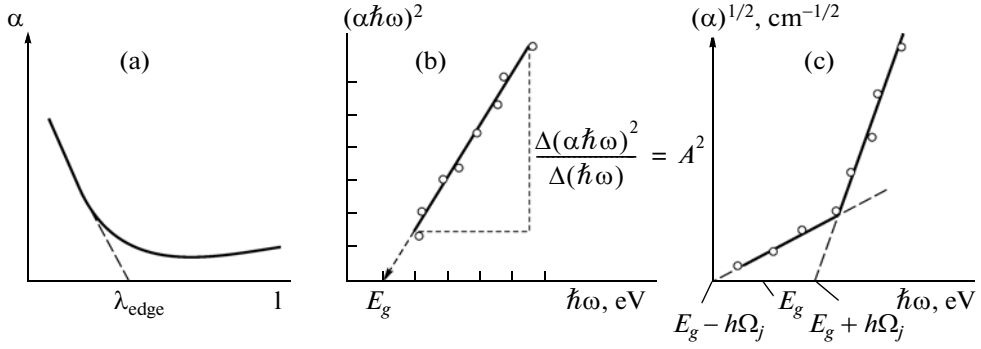

Fig. 4. A scheme for estimating the optical bandgap energy from the dependences of (a) the absorption coefficient α on the wavelength λ of incident light, (b) $(\alpha\hbar\omega)^2$ on $\hbar\omega$, and (c) $\sqrt{\alpha} = f(\hbar\omega)$.

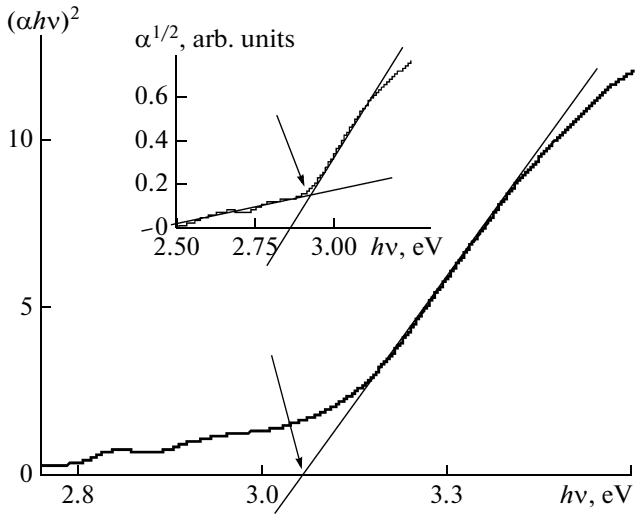

Fig. 5. Graphic estimation of the optical bandgap energy of the pure TiO_2 specimens from the experimentally measured dependences $(\alpha\hbar\omega)^2$ and $\sqrt{\alpha}$ on $\hbar\omega$.

this case, it is possible to use, with the admissible error, the expression

$$T = (1-R)^2\exp(-D),$$

which provides the possibility of calculating the absorption coefficient from the measured R (Fresnel reflection coefficient), T (transmittance), and d as

$$\alpha = \frac{1}{d}\ln\frac{(1-R)^2}{T}.$$

The situation becomes more complicated for the detection of scattered radiation. Although no strict multiple scattering theory exists, the theory of the diffuse reflection and transmission of optically opaque specimens, i.e., the so-called two-component theory developed by Kubelka and Munk in the 1830–1840s, is rather widely applied. For scattering specimens, this theory has the same importance as the Bouguer–Beer law in the absorption spectroscopy of transparent specimens. In this theory, it is assumed that reflected radiation is isotropic, i.e., direction independent, and radiating light is monochromatic.

As a result of the solution of the Kubelka–Munk equation system, it turns out that the diffusion reflectance R_∞ of a specimen depends only on the ratio of the absorption coefficient $K = \alpha$ and the scattering coefficient S instead of either the scattering coefficient or the absorption coefficient, i.e.,

$$K/S = (1-R_\infty)^2/2R_\infty = F(R_\infty).$$

The function $F(R_\infty)$ is called the Kubelka–Munk function.

In diffusion reflection spectroscopy, as well as in absorption and emission spectroscopy, the dependence of the response of an instrument on the wavelength must be eliminated. This is provided by measuring the diffusion reflection spectrum of a specimen itself $\log R(\lambda)$ and the spectrum of scattering from an infinitely reflecting surface $R_{ref}(\lambda)$, for example, from a surface coated with a thin barium sulfate, magnesium carbonate, or magnesium oxide layer; here, their ratio is calculated in the logarithmic form $\log[R(\lambda)/R_{ref}(\lambda)$. In the absence of reflection from the bottom part of a specimen (for example, when a specimen has a sufficient thickness for light to be completely absorbed), it is equal to $\log R_\infty$.

For the practical estimation of the bandgap energy in the case of direct interband transitions, the experimental data are expressed in the form of the dependence

$$(\alpha\hbar\omega)^2 = A^2(\hbar\omega - E_g),$$

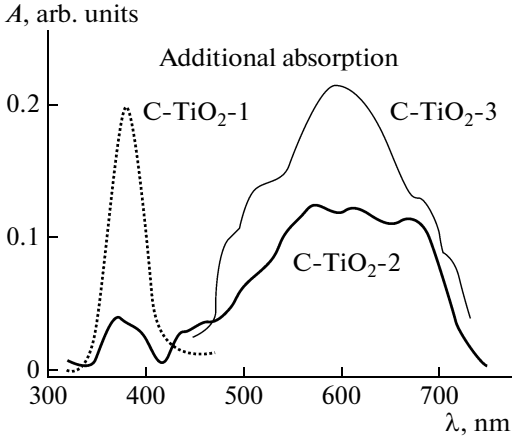

Fig. 6. Spectra of additional absorption produced by the introduction of admixture carbon into titania.

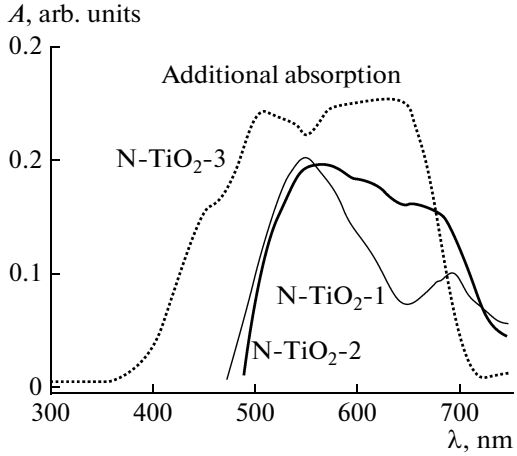

Fig. 7. Spectra of additional absorption produced by the introduction of admixture nitrogen into titania.

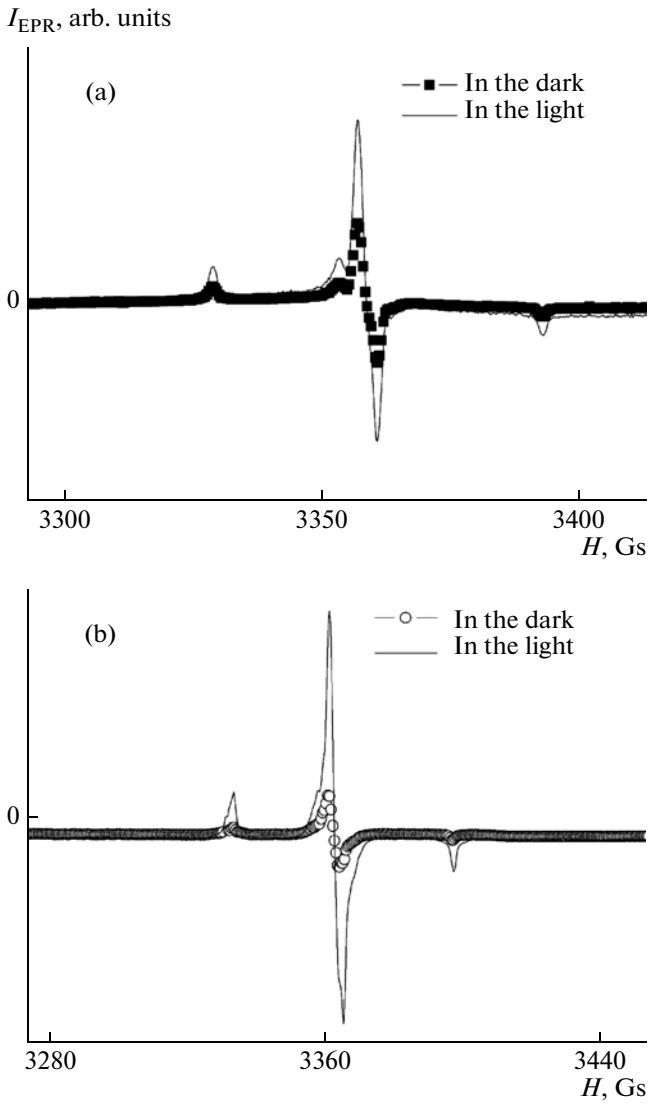

Fig. 8. EPR spectra of the N–TiO_2–3 specimens (a) in the dark and under the radiation with natural light and (b) in the dark and under the radiation with an incandescent lamp. The EPR spectra recording temperature is 300 K.

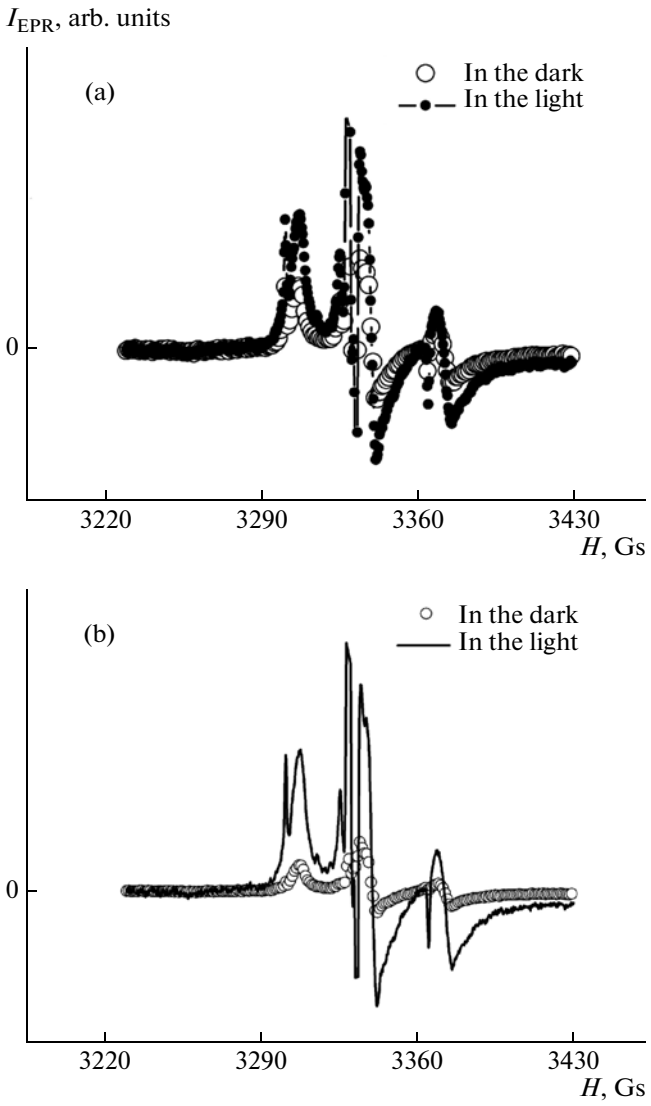

Fig. 9. EPR spectra of the N–TiO_2–3 specimens (a) in the dark and under radiation with natural light and (b) in the dark and under the radiation with an incandescent lamp. The EPR spectra recording temperature is 77 K.

which must be linear (Fig. 4b). As can be seen from Fig. 4b, the value of E_g is determined by extrapolating the linear dependence to the intersection with the abscissa axis.

The experimental results of measuring the dependence of α on $\hbar\omega$ for indirect interband transitions are plotted in the form of curves $\sqrt{\alpha} = f(\hbar\omega)$ (Fig. 4c). Taking the fact into account that $\hbar\Omega_i$ is small in comparison with E_g, it is usually possible to determine the bandgap energy.

We analyzed the measurement results using different methods for the estimation of the bandgap energy. The scheme of the graphical estimation of the direct bandgap energy of a pure TiO_2 specimen, whose scattering spectrum in shown in Fig. 3, is shown in Fig. 5. The scheme for estimating the indirect bandgap energy from a real spectral dependence is demonstrated in the embedding.

The bandgap energy values we obtained using different methods for all the studied materials lie within a range of 2.9–3.2 eV, and are in good agreement with the data for titanium oxides [21–24]. It is important to note that the insertion of admixture nitrogen and carbon did not lead to any considerable change in the bandgap energy of a material. The bandgap energy of a doped material remained the same, with a precision of ±0.1 eV.

We then needed to determine the changes that occur in the visible region of the absorption spectra of TiO_2 specimens after doping with admixtures. To accomplish this, we took corresponding pairs of spec-

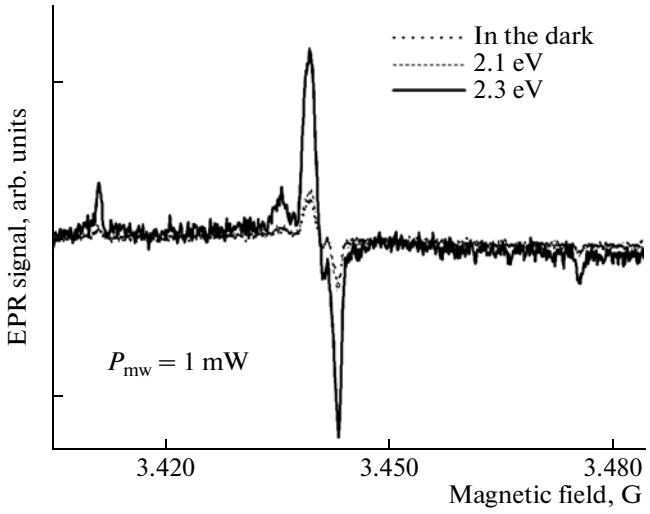

Fig. 10. The EPR spectra of the N–TiO_2–3 specimens in the dark and under the radiation with different-energy quanta.

tra that were obtained from pure titania and a modified material and determined the contribution of the admixtures to the absorption of light by subtracting them from one another. The difference spectra that were obtained from different specimens of the same material were averaged and smoothed. The spectra of additional absorption produced by the introduction of admixture carbon into titania are illustrated in Fig. 6. From Fig. 6 it can be seen that the additional absorption of a material in the visible spectral region grows, as the concentration of the admixture increases.

The spectra of additional absorption of titania due to the introduction of admixture nitrogen to it are shown in the next figure. From Fig. 7 it can be seen that an increase in the amount of admixture nitrogen atoms introduced into titania also increases the absorption coefficient in the visible region. The additional absorption values were normalized to the maximum absorption of pure TiO_2. It is obvious that the integral absorption of each specimen in the visible spectral region is proportional to the area under a corresponding spectrum.

From the results of these optical studies, it is possible to draw the conclusion that the growth of the concentration of both admixture nitrogen and carbon increases the absorption of light by TiO_2 nanoparticles in the visible spectral region, although the energy bandgap of the material remains nearly unchanged.

Further, we studied the effect of photoexcitation with different-energy quanta on the paramagnetic properties of doped nanocrystalline titania specimens. The specimens were radiated with natural light or the light of an incandescent lamp (100 W). The results of radiating the N–TiO_2–3 specimens with natural light indoors and with an incandescent lamp are shown in Figs. 8a and 8b, respectively. As can be seen from this figures, the amplitude of EPR spectra and the radical concentration proportional to it grow under light, and the effect from the photoexcitation with a lamp was more appreciable.

Similar results were also obtained for $NO^{\cdot}$ radicals (Fig. 9).

To determine the positions of the levels of radicals in the bandgap, we performed experiments on the radiation of specimens with different-energy quanta. For this purpose, we used a Bruker Elexsys ER 203 high-pressure mercury lamp (100 w). The required wavelength was separated with an MDR-204 monochromator. The EPR spectra of N–TiO_2–3 specimens in the dark and under radiation with different-energy quanta are shown in Fig. 10. It can be seen that the intensity of the EPR signal abruptly grows at $h\nu$ = 2.3 eV. This effect is illustrated in more detail in Fig. 11. Such variations in the amplitude of the EPR signal from $N^{\cdot}$ radicals can be explained, assuming the existence of extrinsic absorption in the studied specimens according to $N^- + h\nu \longrightarrow N^0 + e$ (on the conduction band). Hence, the number of paramagnetic sites grows. The change of the amplitude of an EPR signal was a completely reversible process. The band

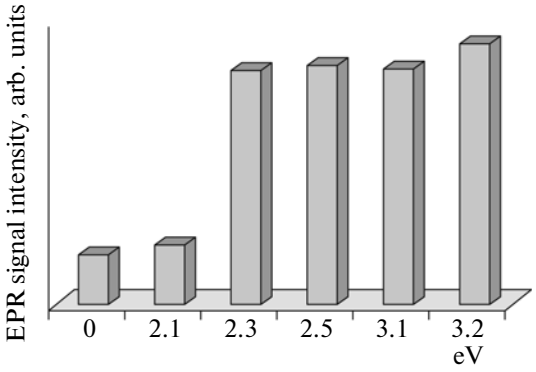

Fig. 11. A diagram of the dependence of the intensity of an EPR signal on the energy of an incident light quantum.

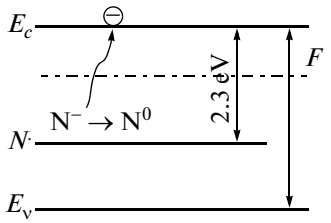

Fig. 12. The band scheme of the process of extrinsic light absorption in N–TiO_2.

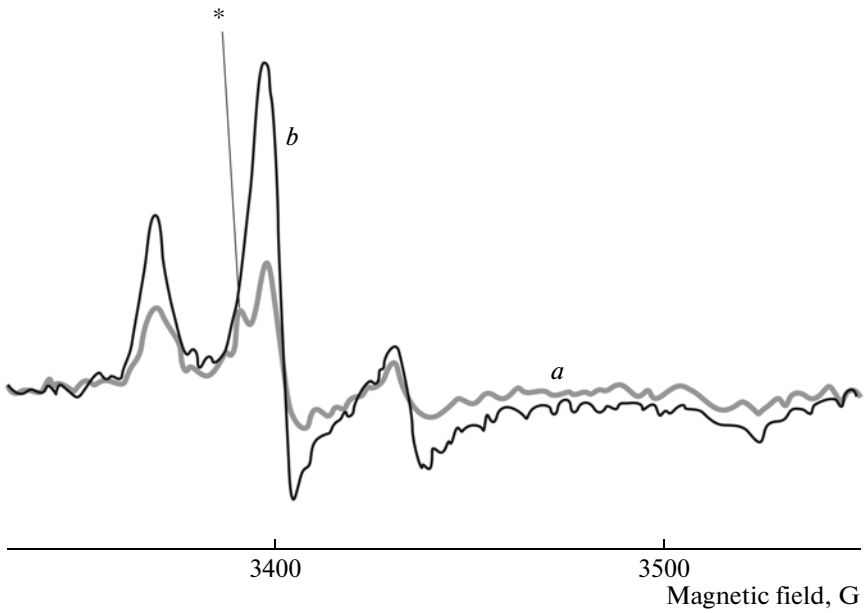

Fig. 13. The transformations of the EPR spectrum of the N–TiO_2–3 specimens at a temperature of 77 K (*a*) before and (*b*) after exposure to light with $h\nu = 2.1$ eV. The asterisk indicates the narrow EPR curve peak produced by $N^{\bullet}$ radicals.

scheme of this process is shown in Fig. 12. The complete reversibility of the effect of light argues for the realization of this process.

We also studied the effect of photoexcitation with different-energy quanta on the behavior of $NO^{\bullet}$ radicals. The amplitude of the EPR signal of $NO^{\bullet}$ radicals and, correspondingly, their concentration, were observed to grow under light with $h\nu = 2.1$ eV (Fig. 13, curve *b*).

Similar measurements were also performed under light with other energies of quanta. The results are shown in Fig. 14.

It may be supposed that an electron passes from the NO^{-} level into the conduction band upon the absorption of a quantum and a site becomes paramagnetic. The process was completely reversible after the light was turned off. The data indicate that the $NO^{\bullet}$ level is nearly 2 eV lower than the bottom edge of the conduction band (Fig. 15).

Similar studies were performed for the carbon-doped nanocrystalline titania specimens. The results of the effect of light on the EPR spectra of this specimens under radiation with natural light and with an incandescent lamp are illustrated in Figs. 16a and 16b, respectively.

As follows from this figure, the EPR-spectra amplitude and the radical concentration, which is proportional to it, grow under light, and the effect is more appreciable in the case of photoexcitation with a lamp and completely reversible. The results of radiating the carbon-containing specimens with different-energy quanta are shown in Fig. 17.

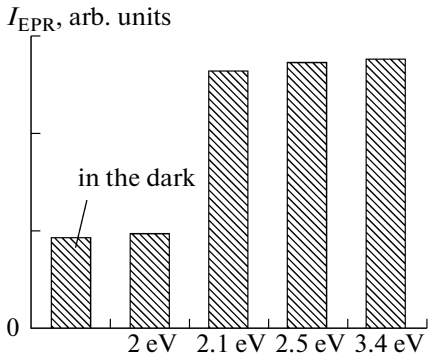

Fig. 14. A diagram of the dependence of the intensity of the EPR signal from $NO^{\bullet}$ radicals on the energy of an incident light quantum.

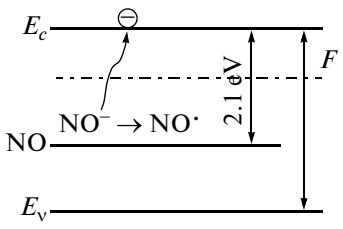

Fig. 15. The process of the photoexcitation of an electron from the $NO^{\bullet}$ level to the conduction band.

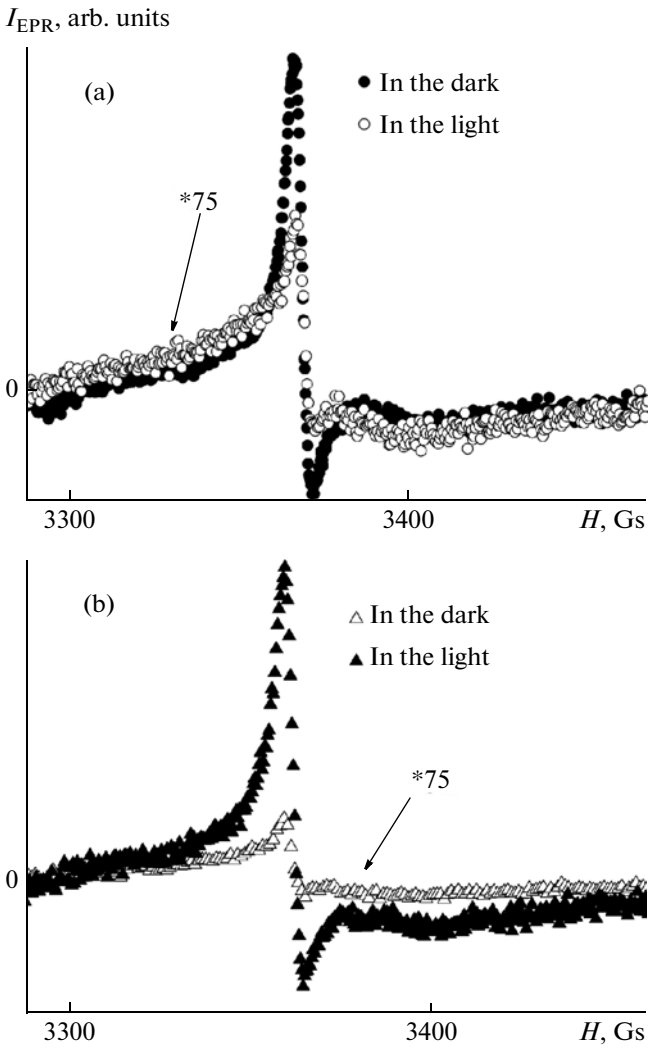

Fig. 16. The EPR spectra of the C–TiO_2–3 specimens (a) in the dark and under the radiation with natural light and (b) in the dark and under the radiation with an incandescent lamp. The EPR spectra recording temperature is 77 K.

These data can be explained by the transition of an electron from the CO_2^{2-} level into the conduction band upon the absorption of a light quantum. As a result, a defect becomes paramagnetic and the amplitude of an EPR signal grows. The CO_2^{2-} level is nearly 2.5 eV lower than the bottom edge of the conduction band.

For all the studied specimens, we calculated the concentrations of N_s radicals, i.e.,

(1) The concentration of all radicals under natural light

$$N–TiO_2–1 – N_s = (2 \pm 0.2) \times 10^{19}\ g^{-1},$$
$$N–TiO_2–2 – N_s = (4.5 \pm 0.5) \times 10^{19}\ g^{-1},$$
$$N–TiO_2–3 – N_s = (1.7 \pm 0.2) \times 10^{20}\ g^{-1},$$

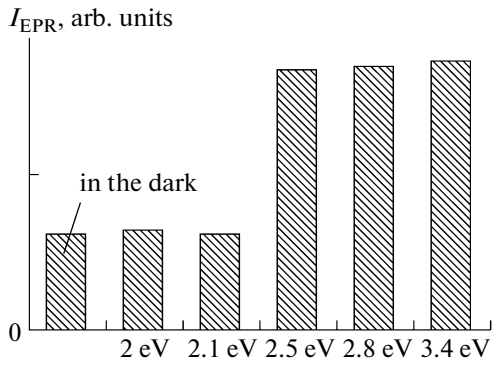

Fig. 17. A diagram of the dependence of the intensity of the EPR signal from CO_2^- radicals on the energy of an incident light quantum.

$$C–TiO_2–1 – N_s = (2 \pm 0.2) \times 10^{17}\ g^{-1},$$
$$C–TiO_2–2 – N_s = (3 \pm 0.5) \times 10^{19}\ g^{-1},$$
$$C–TiO_2–3 – N_s = (1.5 \pm 0.2) \times 10^{20}\ g^{-1},$$

(2) The concentrations of all radicals under the radiation with an incandescent lamp (100 W)

$$N–TiO_2–1 – N_s = (3.5 \pm 0.4) \times 10^{19}\ g^{-1},$$
$$N–TiO_2–2 – N_s = (8.0 \pm 0.8) \times 10^{19}\ g^{-1},$$
$$N–TiO_2–3 – N_s = (3.2 \pm 0.3) \times 10^{20}\ g^{-1},$$
$$C–TiO_2–1 – N_s = (2.2 \pm 0.2) \times 10^{17}\ g^{-1},$$
$$C–TiO_2–2 – N_s = (5.0 \pm 0.5) \times 10^{19}\ g^{-1},$$
$$C–TiO_2–3 – N_s = (2.9 \pm 0.3) \times 10^{20}\ g^{-1}.$$

CONCLUSIONS

(1) The EPR spectra amplitude and the radical concentration proportional to it grow under light and the effect is more appreciable in the case of photoexcitation with a lamp and is completely reversible.

(2) The variations of the amplitude of EPR signals in the dark–light–light source turning off cycles are explained by the processes of the recharge of defect sites.

(3) It was established that the levels of $N^{\bullet}$, $NO^{\bullet}$, and CO_2^- radicals are nearly 2.3, 2.1, and 2.5 eV lower than the bottom edge of the conduction band.

(4) The concentrations of radicals in nitrogen and carbon doped nanocrystalline titania have been calculated. Maximum concentrations are observed in the specimens with the highest admixture content and are $N_s = (1.7 \pm 0.2) \times 10^{20}\ g^{-1}$ (or $(1.5 \pm 0.2) \times 10^{18}\ m^{-2}$) under natural light and $N_s = (3.2 \pm 0.3) \times 10^{20}\ g^{-1}$ (or $(2.8 \pm 0.3) \times 10^{18}\ m^{-2}$) under the radiation with an incandescent lamp for nitrogen-containing specimens and $N_s = (1.5 \pm 0.2) \times 10^{20}\ g^{-1}$ (or $(1.36 \pm 0.14) \times 10^{18}\ m^{-2}$) under natural light and $N_s – (2.9 \pm 0.3) \times 10^{20}\ g^{-1}$ (or $2.6 \pm 0.3) \times 10^{18}\ m^{-2}$ under the radiation

with an incandescent lamp for carbon-containing specimens.

ACKNOWLEDGMENTS

This work was supported by the Ministry of Science and Education within the framework of the Federal Target Program Research and Development in the Priority Fields of the Scientific and Technological Complex of Russia for 2007–2013 (state contract no. 16.513.11.3141) and was performed on the equipment of the Center of Collective Use of Moscow State University.

REFERENCES

1. M. A. Pugachevskii, Tech. Phys. Lett. (Engl. Transl.) **39** (1), 36 (2013).
2. H. C. Choi, H. J. Ahn, Y. M. Jung, et al., Appl. Spectrosc. **58**, 598 (2004).
3. N. Sakai, Y. Ebina, K. Takado, et al., J. Am. Chem. Soc. **126**, 5851 (2004).
4. X. Chen and S. Mao, Chem. Rev. **107**, 2891 (2007).
5. G. Snider and P. Ariya, Chem. Phys. Lett. **491**, 23 (2010).
6. T. Peng, D. Zhao, K. Dai, et al., J. Phys. Chem. B **109**, 4947 (2005).
7. B. S. Richards, Sol. Energy Mater. Sol. Cells **79**, 369 (2003).
8. M. Gratzel, J. Photochem. Photobiol., C **4**, 145 (2003).
9. M. R. Hoffmann, S. T. Martin, W. Choi, et al., Chem. Rev. **95**, 69 (1995).
10. V. M. Zainullina, V. P. Zhukov, V. N. Krasil'nikov, et al., Phys. Solid State (Engl. Transl.) **52** (2), 253 (2010).
11. A. N. Pikhtin and H. H. Hegazy, Semiconductors (Engl. Transl.) **43** (10), 1259 (2009).
12. X. Chen and S. S. Mao, Chem. Rev. **107**, 2891 (2007).
13. Y. Bassekhouad, D. Robert, and J. V. Weber, J. Photochem. Photobiol., A **157**, 47 (2003).
14. G. Oskam, A. Nellore, R. L. Penn, and P. C. Searson, J. Phys. Chem. B **107**, 1734 (2003).
15. T. Sugimoto, X. Zhou, and A. Muramatsu, J. Colloid Interface Sci. **252**, 339 (2002).
16. T. Sugimoto, X. Zhou, and A. Muramatsu, J. Colloid Interface Sci. **259**, 53 (2003).
17. H. Zhang and J. F. Banfield, Chem. Mater. **14**, 4145 (2002).
18. H. Zhang and J. F. Banfield, Chem. Mater. **17**, 3421 (2005).
19. L. Miao, S. Tanemura, S. Toh, et al., J. Cryst. Growth **264**, 246 (2004).
20. P. W. Atkins and M. C. R. Symons, *The Structure of Inorganic Radicals* (Elsevier, Amsterdam, 1967).
21. J. Pascual, J. Camassel, and H. Mathieu, Phys. Rev. B: Condens. Matter Mater. Phys. **18**, 5606 (1978).
22. R. Sanjines, H. Tang, H. Berger, et al., J. Appl. Phys. **75**, 2945 (1994).
23. H. Tang, F. Levy, H. Berger, and P. E. Schmid, Phys. Rev. B: Condens. Matter Mater. Phys. **52**, 7771 (1995).
24. S. D. Mo and W. Y. Ching, Phys. Rev. B: Condens. Matter Mater. Phys. **51**, 13023 (1995).

Translated by E. Glushachenkova